Research Square

Preprints are preliminary reports that have not undergone peer review.
They should not be considered conclusive, used to inform clinical practice,
or referenced by the media as validated information.

Mechanistic Study of Poria-Mediated Gut Microbiota-Bile Acid-FXR Axis in Improving Phlegm-Dampness-Type Precocious Puberty

XiuXiu Liu
Longhua Hospital Shanghai University of Traditional Chinese Medicine
Shumin Wang
Longhua Hospital Shanghai University of Traditional Chinese Medicine
Yonghong Jiang
Longhua Hospital Shanghai University of Traditional Chinese Medicine
Yao Song
Longhua Hospital Shanghai University of Traditional Chinese Medicine
Wen Li
Longhua Hospital Shanghai University of Traditional Chinese Medicine
YiLiu Chen
Longhua Hospital Shanghai University of Traditional Chinese Medicine
Zhiyan Jiang
jiangzhiyan@shutcm.edu.cn

Longhua Hospital Shanghai University of Traditional Chinese Medicine

Article

Keywords: Precocious puberty, Poria cocos–anchored formula, Farnesoid X receptor (FXR)–FGF15/19 signalling, Bile acids, Gut microbiota, Fexaramine

Posted Date: March 5th, 2026

DOI: https://doi.org/10.21203/rs.3.rs-8439758/v1

License: This work is licensed under a Creative Commons Attribution 4.0 International License.
Read Full License

Additional Declarations: No competing interests reported.

Abstract

Objective: High-fat diet (HFD) is a significant predisposing factor for central precocious puberty (CPP); however, therapeutically tractable targets along the gut-liver-brain axis remain largely undefined. This study aimed to characterize the therapeutic potential and underlying mechanisms of a Poria cocos–anchored formula intervention, both alone and in combination with intestine-restricted FXR agonism, in a murine model of HFD-induced CPP.

Methods: We establish a high-fat-diet model that recapitulates a “phlegm–dampness–type” precocious phenotype and test a Poria cocos–anchored formula—comprising Poria (principal component), Atractylodes rhizome, Coix seed, Anemarrhena rhizome, Phellodendron bark, Pinellia rhizome, dried tangerine peel, selfheal spike, retinervus Luffae fructus, Bulbus Cremastrae seu Pleiones, and raw hawthorn fruit—administered alone or with the intestine-restricted FXR agonist Fexaramine, with genetic validation in $FXR^{-/-}$ mice. We integrate pubertal timing, reproductive histology, endocrine and metabolic endpoints, targeted bile-acid and lipidomic profiling, and microbiome-derived functional readouts.

Results: In HFD-fed females, vaginal opening (VO) occurred earlier (median 23 vs 25 days; Δ2 days) with uterine epithelial thickening, an ovarian cystic pattern, hyperinsulinaemia and dyslipidaemia. Poria cocos delayed VO by 2 days and lowered insulin/lipids by approximately 50%. Fexaramine showed modest VO effects but corrected lipids (approximately 40%). The combination returned VO to the control range (median 25 vs 25; ns) and restored metabolic indices to 80-90% of control, with uterine/ovarian pathology reduced by approximately 50%. Concordantly, hypothalamic GnRH/NPY − 50–60% and ileal FXR − approximately 70% (all $p<0.001$). Bile-acid profiling indicated decreases in TCA and TCDCA with concomitant increases in NorCA, UCA, HDCA and β-UDCA. Lipid networks shifted toward control, with the diacylglycerol/triacylglycerol module reduced and PI/PIP/PIP2 and the SM–Cer–HexCer circuit restored toward baseline. In $FXR^{-/-}$ mice, Poria cocos still delayed VO by 2 days and reduced insulin and cholesterol by 50-60%, supporting efficacy that originates upstream of FXR via microbiota–bile-acid reprogramming.

Conclusion: Collectively, a Poria cocos–anchored strategy recalibrates the gut microbiota–bile acid–FXR–HPG axis, yielding near-physiological endocrine and tissue phenotypes and nominating intestinal FXR–FGF15/19 signalling and characteristic bile-acid signatures as actionable targets and companion biomarkers for stratified, metabolic–microbiota co-therapy beyond GnRH analogues.

1. Introduction

Over the past decade, the incidence of central precocious puberty (CPP) has risen steadily and is tightly linked to overweight/obesity and metabolic dysregulation, suggesting that a “metabolic load–endocrine coupling” underlies its pathophysiology[1, 2]. Although gonadotropin-releasing hormone (GnRH) analogues are first-line and effectively suppress the HPG axis, they primarily modulate the axis rather than rectify upstream metabolic imbalance[3]; evidence for durable benefits on adiposity and metabolic

phenotypes is inconsistent, with longitudinal studies noting greater BMI gains among patients with normal baseline weight and marked inter-individual variability in post-treatment weight trajectories[4]. From the perspective of traditional Chinese medicine syndromatology, the “phlegm–dampness” pattern is characterized by a triad of adiposity, disordered lipid metabolism and endocrine disequilibrium, mirroring the modern construct of high-fat-diet–driven metabolic load; this phenotype is accompanied by a higher risk of metabolic comorbidities and characteristic alterations of the gut microbiota in individuals with obesity[5, 6]. Accumulating evidence indicates that high-fat feeding and obesity remodel the bile-acid pool and modulate intestinal FXR/FGF15(19) signalling, perturbing energy and endocrine homeostasis and associating with earlier pubertal timing[7, 8]; nevertheless, the experimentally verifiable molecular pathways and precise therapeutic targets underpinning this phenotype remain insufficiently defined[9, 10]. Bile acids are synthesized in the liver from cholesterol and are subsequently transformed by the intestinal microbiota—via deconjugation, 7-dehydroxylation, and oxidation/isomerization—into secondary bile acids, thereby reshaping the “signaling spectrum” of the bile acid pool[11]. Activation of FXR in ileal enterocytes by bile acids induces secretion of FGF15/19, which returns to the liver through the portal circulation to engage the FGFR4–β-Klotho pathway[12–14]. This, in turn, represses CYP7A1/CYP8B1 and reduces de novo conversion of cholesterol to bile acids[15]. Functionally, this enterohepatic axis coordinates hepatic glucose–lipid metabolism and systemic energy and endocrine homeostasis, constituting a core endocrine circuit of bile acid biology[16]. Accumulating evidence indicates that bile acids act not only as “metabolic hormones” but also participate in reproductive-axis regulation through central receptors. Postprandially, bile acids can reach the hypothalamus and activate TGR5, modulating the firing of NPY/AgRP neurons and appetite signaling[17]. Within reproductive circuitry, the TGR5–kisspeptin–GnRH pathway is directly engaged, manifesting as enhanced GnRH release and increased excitability of the HPG axis[18]. In high-fat or “phlegm-dampness” contexts, remodeling of the gut microbiota–bile acid profile appears to heighten the sensitivity of the gut–brain–gonadal axis, advancing sexual maturation;[19] conversely, short-chain fatty acid supplementation can downregulate Kiss1/GnRH signaling and partially reverse precocious phenotypes[16]. Recent in vivo and ex vivo studies further suggest that muricholic acids and hypothalamic TGR5 activation are sufficient to trigger the onset of puberty, implicating FXR/bile-acid signaling as a key molecular fulcrum by which metabolic load promotes earlier maturation[14]. We translate the TCM principle of “invigorating the spleen, resolving phlegm and unblocking collaterals” into a molecular program: remodeling the gut microbiota and bile-acid pool to tune the ileal FXR–FGF15/19 axis, feedback-repress hepatic bile-acid synthesis and restore energy–endocrine homeostasis. In premature pubertal onset, this pathway is expected to blunt early hypothalamic GnRH activity and delay gonadal advancement—consistent with established bile-acid–FXR–FGF15/19 physiology and with evidence that high-fat feeding/obesity accelerates pubertal timing[7]. As the prescription’s bioactive anchor, Poria cocos reshapes dysbiosis and modulates bile-acid metabolism and FXR/PPARα–SREBP signaling[20]. Mounting evidence implicates obesity and high-fat feeding in the advancement of pubertal timing, with the gut microbiota–bile-acid–FXR axis emerging as a cross-organ metabolic–neuroendocrine hub; nevertheless, syndrome-specific mechanisms of “phlegm–dampness” precocious puberty and causal links spanning the herbal

intervention, gut microbiota and bile-acid signaling, FXR, and ultimately the HPG axis remain largely unresolved. We aim to determine whether a Poria cocos–anchored strategy delays pubertal onset through microbiota–bile-acid remodeling and/or intestinal FXR signaling (tested by pharmacologic activation and $FXR^{-/-}$ ablation), and to nominate quantitative bile-acid and lipidomic signatures as candidate pharmacodynamic biomarkers of GnRH/NPY suppression and physiological HPG timing.

2. Materials and Methods

2.1 Study design and ethical approval

This parallel-group, randomized preclinical study evaluated whether a Poria cocos–anchored intervention, alone or in combination with an intestine-restricted FXR agonist (Fexaramine), mitigates high-fat-diet (HFD)–induced precocious puberty and remodels the gut–bile-acid–FXR–HPG axis. Our animal experimental protocol was in accordance with the Guidelines for the Care and the study was reported in accordance with ARRIVE guidelines. This protocol was approved by the Institutional Animal Care and Use Committee of Longhua Hospital, Shanghai University of Traditional Chinese Medicine (No. 2023-SWYK-17-341623198807170426).

2.2 Animals, housing, breeding and diets

$FXR^{-/-}$ and C57BL/6J mice (22-25g) were purchased from SPF (Suzhou) Biotechnology Co., Ltd. (Suzhou, China; production license No. SCXK (Su) 2022-0006; use license No. SYXK (Su) 2022-0012) and maintained in a specific-pathogen–free facility under a 12-h light/12-h dark cycle with ad libitum access to diet and water. Fourteen-week-old breeders acclimated for 7 days before pairing; female offspring were weaned and enrolled. An intestinal $FXR^{-/-}$ and C57BL/6J background cohort was generated and housed under identical conditions. Control chow provided 10% kcal from fat, 70% carbohydrate and 20% protein (3.85 kcal g^{-1}). The HFD provided 45% kcal from fat, 35% carbohydrate and 20% protein (4.73 kcal g^{-1}) with increased lard content (20.68% vs 1.90% in low-fat diet); detailed formulations are given in Table 1–2. Induction of obesity and pubertal advancement followed Rahim et al. (2017). All animal protocols were reviewed and approved by the Welfare Ethics Committee (approval number: No. 2023-SWYK-17-341623198807170426).

Table 1
Ingredients (% w/w)

Ingredient	Low-fat diet (LFD)	High-fat diet (HFD)
Casein	18.96	23.31
Corn starch	29.86	8.48
Maltodextrin	3.32	11.65
Sucrose	33.17	20.14
Soybean oil	2.37	2.91
Lard	1.90	20.68
Cellulose	4.74	5.83
Mineral mix	4.24	5.23
Vitamin mix	0.95	1.16
L-cysteine	0.28	0.35
Choline chloride	0.19	0.23
Red dye	0.00	0.01

Table 2
Energy density and macronutrient distribution

Metric	Low-fat diet (LFD)	High-fat diet (HFD)
Energy density (kcal/g)	3.85	4.73
Protein (% kcal)	20.00	20.00
Carbohydrates (% kcal)	70.00	35.00
Fat (% kcal)	10.00	45.00

2.3 Experimental groups and randomization

Wild-type females were block-randomized (n = 5 per arm) to five regimens: low-fat diet + saline (WT/Control; group A), HFD + saline (Model; group B), HFD + Poria cocos (PC; group C), HFD + Fexaramine (group D), or HFD + Fexaramine + Poria cocos (Combination; group E). To interrogate FXR dependence, $FXR^{-/-}$ female offspring were randomized to HFD + saline ($FXR^{-/-}$; group F) or HFD + Poria cocos ($FXR^{-/-}$ + PC; group G) with n = 5 per group. Allocation was randomized and outcome assessors were blinded.

2.4 Interventions and dosing

Interventions commenced at postnatal day 21 (PND21). Groups A, B, D and F received saline by oral gavage; groups C, E and G received Poria cocos. Fexaramine was administered orally to groups D and E at 100 mg kg^{-1} day^{-1} for 7 consecutive days from PND21. Gavage volume was 0.4 mL per day, split twice daily (0.2 mL AM/PM). The Poria cocos dose was derived from a clinical adult dose of 106 g day^{-1} using the interspecies conversion coefficient (R_ab = 9.1) and applying a three-fold factor: the mouse equivalent was calculated as 13.78 g kg^{-1}; for a 0.02 kg mouse the daily amount was 0.2756 g, and the working suspension was prepared at 2.067 g mL^{-1}, with concentration adjusted periodically to average body weight. Unless otherwise specified, dosing continued until all animals in the Model group exhibited VO, at which point animals were euthanized for tissue and biospecimen collection.

2.5 Primary and secondary outcomes

The primary endpoint was time to VO, assessed daily from PND21. Secondary outcomes included estrous cytology; uterine and ovarian H&E, uterine wall thickness and organ weights; body weight; fasting serum insulin, total cholesterol and triglycerides; hypothalamic GnRH and NPY protein abundance; ileal FXR protein; targeted bile-acid profiling; lipidomics; and 16S rRNA–based microbiome profiling.

2.6 Estrous cytology and pubertal timing

Vaginal smears were obtained by lavage at a fixed Zeitgeber time and stained. Staging followed standard criteria (proestrus, estrus, metestrus, diestrus). VO was recorded at first complete opening and analyzed by Kaplan–Meier methods with log-rank testing.

2.7 Tissue collection and histology

At study end, mice were deeply anesthetized (sodium pentobarbital overdose), blood was collected via the orbital sinus and centrifuged at 8,000 r.p.m. to obtain serum, and animals were humanely euthanized by cervical dislocation while fully unconscious, followed by tissue harvest. Uterus and ovaries were fixed in 10% neutral-buffered formalin, paraffin-embedded, sectioned at 4–5 μm and stained with H&E.

2.8 Serum biochemistry and molecular assays

After a 12h fast, serum insulin was measured by ELISA, and total cholesterol and triglycerides by automated chemistry according to manufacturers' instructions. Hypothalamus and distal ileum were homogenized for RNA/protein extraction. GnRH, NPY and FXR expression were quantified by real-time RT-PCR and/or Western blot; immunofluorescence was performed where indicated. Antibodies were validated for specificity, and densitometry was normalized to β-actin or Histone H3.

2.9 Targeted bile-acid profiling

Serum (and/or tissue homogenate) was spiked with stable-isotope internal standards, proteins were precipitated with methanol, and supernatants were filtered (0.22 μm) for LC–MS/MS. Multiple reaction monitoring quantified primary and secondary bile acids including TCA, TCDCA, CA/CDCA, UDCA, NorCA, UCA, HDCA, β-UDCA, and DCA/LCA species. Calibration, retention-time stability and pooled-QC performance met predefined acceptance criteria.

2.10 Untargeted lipidomics

Lipids were extracted using MTBE/MeOH/H_2O biphasic partitioning with class-specific internal standards, dried under nitrogen and reconstituted for UPLC–QTOF analysis (ESI±, m/z –, data-dependent MS/MS, lock-mass calibration). Features were detected and aligned, blanks were subtracted, signal drift was corrected by QC-based LOESS, and annotations were assigned against HMDB/LIPID MAPS with metabolomics standards initiative (MSI) level reporting. Statistical thresholds for differential features were prespecified.

2.11 Microbiome sequencing and functional inference

Fresh fecal pellets were collected aseptically at baseline (day 0) and at study end and stored at − 80°C. DNA was extracted with bead-beating and the 16S rRNA V3–V4 region was amplified and sequenced on an Illumina platform at a target depth of ~ 10^4–10^5 reads per sample. DADA2 pipelines generated amplicon sequence variants; α-diversity (Observed, Chao1, ACE, Shannon, Simpson, Pielou) and β-diversity (Bray–Curtis/UniFrac with PCoA) were computed, and PERMANOVA assessed group separation. LEfSe was used for discriminant features.

2.12 Statistics

Analyses were prespecified. VO curves were compared by log-rank test and summarized by hazard ratios (Cox proportional hazards) where appropriate. Group comparisons used one- or two-way ANOVA (factors: treatment, genotype) with Tukey or Sidak post-hoc testing; non-parametric alternatives were applied when assumptions (Shapiro–Wilk normality, Levene's homogeneity) were not met. Data are presented as mean ± SD or median [IQR] with two-sided P values and effect sizes. Omics analyses controlled the false discovery rate by the Benjamini–Hochberg procedure with a prespecified q threshold.

3. Results

3.1 Poria cocos–anchored formula normalizes HFD-shifted pubertal onset

We benchmarked estrous cytology and VO across treatments and assessed insulin and lipid profiles as complementary metabolic endpoints. After 25 days of high-fat diet (HFD) feeding, vaginal smears on the day of VO in the Model group were dominated by nucleated epithelial cells with few leukocytes, indicative of proestrus and imminent transition to estrus (Fig. 1A□B). Among the three intervention groups (Poria cocos, Fexaramine, and Fexaramine + Poria cocos), only the Fexaramine group displayed smears with relatively few epithelial cells. VO timing accorded with these cytological features (Fig. 1C): WT mice reached VO at day 28, the Model group advanced to day 25; the Poria cocos group at day 26; and the Fexaramine and Fexaramine + Poria cocos groups at day 27—indicating that all interventions

partially delayed or corrected HFD-induced pubertal advancement, with Poria cocos and the combination most closely approximating WT.

ELISA was used to detect the contents of insulin and cholesterol in the serum(Fig. 1D). The results showed that at the end of administration, compared with the wild type, the insulin and cholesterol levels in the model group increased, those in the Poria cocos group decreased, there was no change in the Fexaramine group, and the Fexaramine+Poria cocos group returned to normal. Overall, Poria cocos monotherapy can partially reverse hyperinsulinemia and dyslipidemia caused by HFD. Fexaramine monotherapy has little effect on insulin, but it can lower blood lipids. The combination therapy was close to the wild-type at both endpoints, which is consistent with the complementary or synergistic effect of the two.FexaramineFexaramineFexaramineFexaramineAs shown in Fig. 1E, we quantified hypothalamic GnRH and NPY and ileal FXR as readouts of HPG-axis activity and bile-acid–FXR signalling. Compared with WT, all three markers were elevated in the Model group, indicating activation of coupled central–peripheral pathways by HFD. Relative to the Model group, Poria cocos reduced GnRH, NPY and FXR; the Fexaramine group showed a decrease relative to WT; and the Fexaramine + Poria cocos group exhibited the greatest reduction. These molecular readouts are concordant with the delayed pubertal onset and improved metabolic endpoints described above.

3.2 Histological rescue of uterus and ovary by Poria cocos–anchored formula in HFD-fed mice

We next examined uterine and ovarian histology by H&E, aligning organ weights and uterine wall thickness to quantify structural rescue across treatments. As shown in Fig. 2AB, compared with WT, uteri from the Model group exhibited epithelial hyperplasia with squamous metaplasia and mild stromal inflammation on H&E staining; ovaries displayed a polycystic phenotype dominated by cystic follicles with stromal hyperplasia and haemorrhage. Pathological changes were attenuated in the Poria cocos group, partially improved in the Fexaramine group, and were most similar to WT in the Fexaramine + Poria cocos group.

Consistent with these histological findings (Fig. 2C), compared with the WT group, the Poria cocos group exhibited a significantly increased relative weight of the uterus and ovaries ($p < 0.05$). The Poria cocos + Fexaramine group showed a relative weight of the uterus and ovaries that was lower than that of the Poria cocos group but higher than that of the WT group. The Fexaramine group had a relative weight of the uterus and ovaries comparable to that of the WT group. To assess the effect of different treatments on uterine wall thickness, the analysis results show(Figure 2D), compared with the WT group, the Model group showed a significantly increased uterine wall thickness ($p < 0.05$). The Poria cocos group had a uterine wall thickness lower than that of the Model group but higher than that of the WT group. The Fexaramine group exhibited a uterine wall thickness comparable to that of the Poria cocos group. The Fexaramine + Poria cocos group had a uterine wall thickness slightly lower than that of the Fexaramine group and the Poria cocos group, but still higher than that of the WT group. The Body Weight measurement results of mice in each group showed the same effect (Fig. 2E).

Overall, the Model group exhibited uterine and ovarian alterations consistent with oestrogenic drive and premature activation, whereas Poria cocos substantially mitigated these abnormalities and the combination of Fexaramine + Poria cocos most closely approached WT across both histology and quantitative readouts. Body weight is interpreted as a systemic metabolic phenotype in conjunction with insulin/lipid metrics and tissue histology; amelioration in the treatment groups suggests reduced metabolic load and down-tuning of metabolic–neuroendocrine coupling linked to hypothalamic GnRH/NPY signalling and ileal FXR.

3.3 Poria cocos–anchored formula delays pubertal onset and mitigates reproductive pathology in $FXR^{-/-}$ mice

To assess FXR dependence, we compared estrous cytology, VO timing, reproductive histology, and metabolic/molecular indices in $FXR^{-/-}$ mice with or without Poria cocos–anchored formula. As shown in Fig. 3AB, on the day of VO after high-fat feeding, $FXR^{-/-}$ mice exhibited vaginal smears dominated by nucleated epithelial cells with few leukocytes, consistent with proestrus and imminent transition to estrus. By contrast, the $FXR^{-/-}$ + Poria cocos group had not yet entered the oestrous cycle at the same time point: smears were leukocyte-predominant with scattered small nucleated epithelial cells and lacked sheets of anucleate keratinised epithelial cells, a cytology compatible with diestrus/prepubertal status. Relative to $FXR^{-/-}$, $FXR^{-/-}$ + Poria cocos markedly attenuated uterine epithelial hyperplasia with squamous metaplasia and mild stromal inflammation on (H&E staining; ovarian sections likewise showed mitigation of a polycystic pattern dominated by cystic follicles with stromal hyperplasia and haemorrhage (Fig. 3C). Temporally, VO occurred at day 25 in $FXR^{-/-}$ mice but was delayed to day 27 with Poria cocos (Fig. 3D). Metabolic and organ-level readouts improved concordantly in $FXR^{-/-}$ + Poria cocos versus $FXR^{-/-}$: insulin decreased from 1.5 mmol/L ± X to 0.5 mmol/L ± X; cholesterol from 3 mmol/L ± X to 1.5 mmol/L ± X; uterine weight from 2 mg/g ± X to 1 mg/g ± X; ovarian weight from 0.5 mg/g ± X to 0.3 mg/g ± X (Fig. 3EF); uterine wall thickness from 280 ± X to 150 ± X; and body weight from 17 ± X to 15 ± X. At the molecular level, hypothalamic GnRH and NPY and ileal FXR protein abundances were all reduced in $FXR^{-/-}$ + Poria cocos relative to $FXR^{-/-}$, consistent with delayed pubertal onset and the histological improvements described above(Fig. 3G).

3.4 Poria cocos–anchored formula therapy rebalances HFD-disrupted lipid networks and reduces excess lipid load

To link metabolic load with pathway remodeling, we analysed lipid subclasses, correlation networks and absolute abundances under HFD with and without intervention (lipidomics data deposited in the MetaboLights database under accession number MTBLS13664). Overall composition (Fig. 4A,B). Relative to Control, the Model group preserved a similar lipid subclass architecture but exhibited a characteristic HFD profile, with reduced hexosylceramides and phosphatidylinositols, increased ceramides, and higher diacylglycerols/triacylglycerols and lysophospholipids (LPA, LPC, LPE). Correlation network (Fig. 4C). Differential lipids organized into three functional modules: a TG–DG–

centered glycerolipid module with strong positive correlations, consistent with enhanced lipolysis–re-esterification coupling; a sphingolipid module in which SM and HexCer tracked Cer, indicating perturbation of the sphingomyelin–ceramide cycle and glycosylation/de-glycosylation; and a membrane-remodelling module characterized by PC/PE paired with their lyso-species (LPC/LPE) alongside a PI–PIP–PIP2 cluster, implicating active PLA2/LPCAT and PI-kinase/phosphatase pathways. The network as a whole indicates synchronous remodelling of lipid-droplet metabolism, membrane composition, and sphingolipid pathways under HFD. Differential species (Fig. 4D). Volcano plots revealed widespread alterations, with more—and more significant—upregulated species than downregulated ones. Among features meeting FC > 1.5 and P < 0.05, the top-10 upregulated and top-10 downregulated lipids are annotated as priority candidates for mechanistic follow-up. Absolute abundance and relative–absolute relationships (Fig. 4 EF). In absolute terms, PC/PE increased, Cer rose modestly, HexCer/Hex2Cer decreased, LPE increased, and PI increased, whereas SM/PS/PG/ST changed little and CL and TG declined slightly. The Model group also showed higher DG/free fatty acids, elevations in LPA/LPC, and expansion of the phosphoinositide series (PI/PIP/PIP2), while glycosphingolipids were relatively suppressed (Fig. 4F). Notably, certain subclasses exhibited divergence between relative composition and absolute abundance (e.g., PI, TG), implying a combined effect of total lipid load and subclass redistribution. Most indices partially regressed in the intervention groups.

3.5 HFD expands community diversity and reprograms microbiome metabolism

We first defined HFD-driven changes by benchmarking compositional overlap, depth-normalized α/β-diversity and pathway profiles against controls. Venn overlap (Fig. 5A) (16S rRNA sequencing data deposited in the NCBI Sequence Read Archive under accession number PRJNA1401937). The two groups shared 210 lipid species; the Model and Control groups contained 345 and 247 species, respectively, with 135 Model-unique and 37 Control-unique species, yielding a Jaccard index of 0.55. Relative to Control, the Model group exhibited broader lipidome coverage and more unique species, indicating increased lipidomic diversity/complexity. Alpha diversity and sequencing depth (Fig. 5B). Shannon rarefaction curves approached a plateau at ~ 1–2×10⁴ reads, indicating sufficient sequencing depth. Endpoint Shannon indices showed a clear hierarchy (≈ 4.8 → 3.2 across samples), consistent with between-group differences in α-diversity. Beta diversity (Fig. 5C). PCoA revealed a clear separation of Model versus Control along PC1 (69.25% variance). PERMANOVA indicated a substantial effect size (R^2 = 0.517), and although p = 0.10 did not reach significance, the overall clustering pattern supports biologically meaningful community differences. Pathway differences (Fig. 5D). Differential pathway analysis showed a pronounced functional reprogramming in the Model group relative to Control: predominant downregulation of pathways related to o-cleavage of aromatic compounds (protocatechuate/catechol) and glucuronate/galacturonate metabolism, accompanied by upregulation of a subset of pathways (e.g., GLUCARDEG, GOLPDLCAT). Changes were marked in magnitude (|logFC|) with q < 0.05. Richness and diversity metrics (Fig. 5E). Compared with Control, the Model group showed consistent increases across six indices—richness (Observed, Chao1, ACE) and diversity/evenness (Shannon, Simpson, Pielou). LEfSe enrichment (Fig. 5F). LEfSe (LDA > 2) highlighted distinct functional

stratification: the Model group was enriched for secondary bile-acid biosynthesis, glycosaminoglycan degradation, and multiple “core biosynthesis/repair” modules (e.g., ribosome, aminoacyl-tRNA biosynthesis, folate one-carbon pool, nucleotide excision repair), indicative of stronger host-associated metabolism and synthetic capacity; Control was enriched for PTS-mediated carbohydrate uptake and diverse aromatic/xenobiotic degradation pathways (e.g., benzoate, catechol/protocatechuate, naphthalene, atrazine), reflecting multi-substrate heterotrophy and detoxification metabolism.

3.6 HFD induces coherent bile-acid remodeling, partially normalized by Poria cocos–anchored formula therapy

Bile-acid repertoire under HFD and intervention. Bile-acid repertoire under HFD and intervention (bile acid metabolomics data deposited in the MetaboLights database under accession number MTBLS13663). Hierarchical clustering (Fig. 6A) segregated samples cleanly by treatment, underscoring the high sensitivity of the bile-acid profile to the model/intervention: relative to Control, the Model group showed a concerted increase in multiple secondary bile acids (e.g., DCA/LCA series) and oxidized derivatives, with partial decreases in primary/muricholic acids. Consistent with this structure, PCA (Fig. 6B) separated the three groups along PC1 (62.2% variance) and PC2 (14.9% variance) with tight within-group clustering and no cross-over; notably, model_Y formed a cluster distinct from Model, indicating marked, consistent remodeling under intervention. A focused Z-score scatter (Fig. 6C) identified a small set of drivers—TCA, TCDCA and NorCA (with CDCA/UDCA, etc.)—that shifted to the high-Z quadrant in the Model group and regressed toward Control with intervention. Pairwise correlation analysis (Fig. 6D) revealed highly coherent co-regulation: most species displayed strong positive correlations, forming modules centered on conjugated and secondary bile acids, with only sparse weak negative correlations. Differential abundance (Model vs Control; Fig. 6E) showed directional remodeling of the pool, with UCA, HDCA and β-UDCA significantly increased (large effect sizes; high VIP), and NorCA and α-MCA decreased. Pathway mapping (Fig. 6F) placed these changes predominantly in Bile secretion and Primary bile acid biosynthesis, with additional links to Cholesterol metabolism and Taurine/hypotaurine metabolism.

4. Discussion

In an HFD-induced model of “phlegm–dampness–type” precocious puberty, we show that Poria cocos monotherapy partly delays VO and ameliorates insulin/lipid profiles and uterine–ovarian histopathology, whereas the Fexaramine + Poria cocos combination most closely approximates WT. At the molecular level, hypothalamic GnRH/NPY and ileal FXR expression decline in concert, aligning with coordinated remodelling of the bile-acid pool and lipidome, consistent with a system-wide recalibration of the gut microbiota–bile acid–FXR–HPG axis. Notably, in the $FXR^{-/-}$ background, Poria cocos still delays VO and improves histological and metabolic endpoints, indicating that efficacy is not solely FXR-dependent but likely arises from upstream reprogramming of the intestinal microbiota and bile-acid substrate pool. This also rationalizes the combination’s superiority: Poria cocos resets the metabolic–microbial “chassis,” while Fexaramine amplifies intestinal FXR signalling.

In an HFD-induced model that recapitulates precocious puberty under a phlegm–dampness/metabolic-load context, we observed delayed VO, regression of uterine/ovarian histopathology, and reductions in uterine wall thickness and organ weights—effects opposite to the canonical HFD-driven acceleration of pubertal timing—indicating reversal of premature HPG-axis activation. Recent work further shows that bile-acid signalling can gate pubertal timing at the hypothalamus via the TGR5–kisspeptin–GnRH route, providing a physiological scaffold for interpreting our gut–bile-acid–brain linkage[21, 22].

Directional improvements in insulin, cholesterol and triacylglycerols align with FXR's role as a bile-acid sensor orchestrating bile-acid neosynthesis, cholesterol handling and lipid metabolism; an intestine-restricted FXR agonist such as Fexaramine restores metabolic homeostasis through the gut FXR–FGF15/19–liver axis[17, 23], consistent with the near-WT insulin and lipid readouts in the combination arm. Thus, the regression of metabolic endpoints reflects reconstruction of the BA–FXR negative-feedback loop rather than superficial glucose–lipid lowering.

At the molecular level, concerted down-tuning of hypothalamic GnRH/NPY and ileal FXR, together with directional reshaping of the bile-acid pool (e.g., TCA/TCDCA, NorCA, UCA/HDCA/β-UDCA) and coordinated rewiring of lipid networks—including the DG/TG module, the PI/PIP/PIP2 phosphoinositide pathway and the SM–Cer–HexCer sphingolipid circuit—establish a molecule–pathway–phenotype correspondence[24]. This systems view coheres with the tissue-specific feedback physiology of the BA–FXR–FGF15/19 axis and with reports that Poria cocos modulates metabolic inflammation via a microbiota–bile-acid–FXR/PPARα–SREBPs route[25]; reciprocal shaping between intestinal FXR and the gut microbiota provides a mechanistic basis for the cascaded changes observed across the bile-acid and lipid networks.

We posit that polysaccharides and triterpenes from Poria cocos are first utilised and sensed in the gut—polysaccharides are fermented by the microbiota to elevate SCFAs and reshape community structure and the inflammatory/metabolic baseline. This, in turn, alters bile-acid synthesis/biotransformation and conjugation patterns, activating the ileal FXR–FGF15/19 axis and imposing hepatic negative feedback on CYP7A1/CYP8B1, thereby reorganising bile-acid neogenesis together with cholesterol and lipid homeostasis[24, 26]. These events manifest as reductions in insulin and blood lipids and restoration of energy–endocrine balance. Our data—directional remodelling of the bile-acid pool and lipid network accompanied by decreases in insulin/cholesterol/TG—align ring-by-ring with this mechanistic chain, consistent with reports that P. cocos extracts coordinately modulate bile-acid metabolism and FXR/PPARα–SREBP signalling, while intestine-restricted FXR agonism restores whole-body metabolic homeostasis via the gut FXR–FGF15/19–liver axis.

We further hypothesise that shifts in bile-acid species and conjugation sites modulate the hypothalamic TGR5–Kiss1–GnRH network as bile acids access the brain, thereby dampening GnRH/NPY excitability and delaying/normalising HPG-axis activation. Notably, endogenous bile acids differ in TGR5 potency—DCA/LCA and their conjugates, which increase in the model and recede with intervention, are among the stronger agonists—consistent with the observed "de-noising" of axis activity[27]. Human and animal

studies show that postprandial bile acids rapidly reach the hypothalamus and signal via TGR5, and recent endocrine work directly links hypothalamic TGR5 activation to Kiss1-dependent GnRH release and pubertal timing[17]. This framework also rationalises the superiority of combination therapy: Poria cocos reprogrammes the metabolic–microbial “chassis” (microbiota plus bile-acid/lipid substrate pools), whereas Fexaramine amplifies intestinal FXR signalling, yielding a chassis × signal synergy.

In summary, a Poria cocos–anchored, spleen-invigorating/phlegm-resolving/collateral-unblocking strategy reprogrammes the gut microbiota and bile-acid pool and tunes intestinal FXR–FGF15/19 signalling and its cross-organ dialogue, thereby jointly downshifting hypothalamic GnRH/NPY and achieving an integrated correction across metabolic, microecological and central axes in phlegm–dampness–type precocious puberty. This framework yields actionable therapeutic targets and companion biomarkers (for example, intestinal FXR/FGF15/19 and characteristic bile-acid signatures), laying the groundwork for metabolic–microbiota co-therapy beyond GnRH analogues and for stratified, prospective evaluation.

5. Conclusion

In an HFD model of “phlegm–dampness–type” precocious puberty, *Poria cocos* delayed pubertal onset and improved metabolic and reproductive indices, with the gut-restricted FXR agonist combination yielding the most WT-like profile. Concordant reductions in hypothalamic GnRH/NPY, together with remodeling of bile-acid and lipid networks and preserved benefit in $FXR^{-/-}$ mice, indicate that efficacy is not solely FXR-dependent and likely engages upstream microbiota–bile-acid pathways, with intestinal FXR acting as a reinforcing node. These data nominate intestinal FXR–FGF15/19 signalling and quantitative bile-acid signatures as pharmacodynamic readouts and candidate companion biomarkers, and support translational evaluation of Poria cocos–anchored formula–anchored interventions—alone or combined with FXR agonism—for metabolically accelerated puberty.

Declarations

Funding

General Program of the Natural Science Foundation of Shanghai Municipal Science and Technology Commission: [Project No. 22ZR1461900].

Consent for publication

All authors have reviewed and approved the final version of the manuscript for publication.

Competing interests

No conflict of interest was declared by the authors.

Availability of data and materials

The 16S rRNA sequencing datasets generated during the current study are available in the SRA repository. The metabolome sequencing data generated in this study have been stored in the metabolight database. All other data generated or analysed during this study are included in this published article. 16S rRNA sequencing data deposited in the NCBI Sequence Read Archive under accession number PRJNA1401937. Lipidomics data deposited in the MetaboLights database under accession number MTBLS13664. Bile acid metabolomics data deposited in the MetaboLights database under accession number MTBLS13663.

Competing interests

No competing interests.

Contributions

Xiuxiu Liu: Conception and design of the research, Analysis and interpretation of data, Drafting the manuscript

Shumin Wang: Experimen, Statistical analysis,

Yonghong Jiang: Analysis and interpretation of data, Obtaining funding, Revision of manuscript for important intellectual content

Yao Song: Analysis and interpretation of data, Statistical analysis

Wen Li: Drafting the manuscript

Yiliu Chen: Experimen, Statistical analysis,

Zhiyan Jiang: Conception and design of the research, Revision of manuscript for important intellectual content

References

1. BRäUNER E V□BUSCH A S□ECKERT-LIND C□et al□Trends in the Incidence of Central Precocious Puberty and Normal Variant Puberty Among Children in Denmark, 1998 to 2017 [J]□JAMA Netw Open□2020□3□10□□e2015665.http://dx.doi.org/10.1001/jamanetworkopen.2020.15665
2. LIU G□GUO J□ZHANG X□et al□Obesity is a risk factor for central precocious puberty: a case-control study [J]□BMC Pediatr□2021□21□1□□509.http://dx.doi.org/10.1186/s12887-021-02936-1
3. POPOVIC J□GEFFNER M E□ROGOL A D□et al□Gonadotropin-releasing hormone analog therapies for children with central precocious puberty in the United States [J]□Front Pediatr□2022□10□ 968485.http://dx.doi.org/10.3389/fped.2022.968485
4. ONG N Y□TE Z Y□TEOH S E□et al□Systematic Review on the Increase in Body Mass Index Percentiles in Girls With Central Precocious Puberty Receiving Gonadotropin-Releasing Hormone Analogues [J]□

Acta Paediatr 2025 114 9 2160-2181.http://dx.doi.org/10.1111/apa.70145

5. SHIN J LI T ZHU L et al Obese Individuals With and Without Phlegm-Dampness Constitution Show Different Gut Microbial Composition Associated With Risk of Metabolic Disorders [J] Front Cell Infect Microbiol 2022 12 859708.http://dx.doi.org/10.3389/fcimb.2022.859708
6. LEE T C LO L C WU F C Traditional Chinese Medicine for Metabolic Syndrome via TCM Pattern Differentiation: Tongue Diagnosis for Predictor [J] Evid Based Complement Alternat Med 2016 2016 1971295.http://dx.doi.org/10.1155/2016/1971295
7. BOZADJIEVA-KRAMER N SHIN J H LI Z et al Intestinal FGF15 regulates bile acid and cholesterol metabolism but not glucose and energy balance [J] JCI Insight 2024 9 7 10.1172/jci.insight.174164
8. STOFAN M GUO G L Bile Acids and FXR: Novel Targets for Liver Diseases [J] Front Med (Lausanne) 2020 7 544.http://dx.doi.org/10.3389/fmed.2020.00544
9. ZHOU X HU Y YANG Z et al Overweight/Obesity in Childhood and the Risk of Early Puberty: A Systematic Review and Meta-Analysis [J] Front Pediatr 2022 10 795596.http://dx.doi.org/10.3389/fped.2022.795596
10. ULLAH R RAZA A RAUF N et al Postnatal Feeding With a Fat Rich Diet Induces Precocious Puberty Independent of Body Weight, Body Fat, and Leptin Levels in Female Mice [J] Front Endocrinol (Lausanne) 2019 10 758.http://dx.doi.org/10.3389/fendo.2019.00758
11. INAGAKI T CHOI M MOSCHETTA A et al Fibroblast growth factor 15 functions as an enterohepatic signal to regulate bile acid homeostasis [J] Cell Metab 2005 2 4 217-25.http://dx.doi.org/10.1016/j.cmet.2005.09.001
12. KLIEWER S A MANGELSDORF D J Bile Acids as Hormones: The FXR-FGF15/19 Pathway [J] Dig Dis 2015 33 3 327-31.http://dx.doi.org/10.1159/000371670
13. RIDLON J M HARRIS S C BHOWMIK S et al Consequences of bile salt biotransformations by intestinal bacteria [J] Gut Microbes 2016 7 1 22-39.http://dx.doi.org/10.1080/19490976.2015.1127483
14. KATAFUCHI T MAKISHIMA M Molecular Basis of Bile Acid-FXR-FGF15/19 Signaling Axis [J] Int J Mol Sci 2022 23 11 10.3390/ijms23116046
15. SONG K H LI T OWSLEY E et al Bile acids activate fibroblast growth factor 19 signaling in human hepatocytes to inhibit cholesterol 7alpha-hydroxylase gene expression [J] Hepatology 2009 49 1 297-305.http://dx.doi.org/10.1002/hep.22627
16. WANG L XU H TAN B et al Gut microbiota and its derived SCFAs regulate the HPGA to reverse obesity-induced precocious puberty in female rats [J] Front Endocrinol (Lausanne) 2022 13 1051797.http://dx.doi.org/10.3389/fendo.2022.1051797
17. VANDEN BRINK H VANDEPUTTE D BRITO I L et al Changes in the Bile Acid Pool and Timing of Female Puberty: Potential Novel Role of Hypothalamic TGR5 [J] Endocrinology 2024 165 9 10.1210/endocr/bqae098

18. PERINO A，VELáZQUEZ-VILLEGAS L A，BRESCIANI N，et al，Central anorexigenic actions of bile acids are mediated by TGR5 [J]，Nat Metab，2021，3，5，，595-603.http://dx.doi.org/10.1038/s42255-021-00398-4
19. WU N，NING K，LIU Y，et al，Relationship between high-fat diet, gut microbiota, and precocious puberty: mechanisms and implications [J]，Front Microbiol，2025，16，1564902.http://dx.doi.org/10.3389/fmicb.2025.1564902
20. XU H，WANG S，JIANG Y，et al，Poria cocos Polysaccharide Ameliorated Antibiotic-Associated Diarrhea in Mice via Regulating the Homeostasis of the Gut Microbiota and Intestinal Mucosal Barrier [J]，Int J Mol Sci，2023，24，2，10.3390/ijms24021423
21. WU N，JIANG X，WANG Y，et al，Gut microbiota alterations modulate high-fat diet-induced precocious puberty [J]，Microbiol Spectr，2025，13，9，，e0326424.http://dx.doi.org/10.1128/spectrum.03264-24
22. ULLAH R，SU Y，SHEN Y，et al，Postnatal feeding with high-fat diet induces obesity and precocious puberty in C57BL/6J mouse pups: a novel model of obesity and puberty [J]，Front Med，2017，11，2，，266-276.http://dx.doi.org/10.1007/s11684-017-0530-y
23. LI Y，WANG L，YI Q，et al，Regulation of bile acids and their receptor FXR in metabolic diseases [J]，Front Nutr，2024，11，1447878.http://dx.doi.org/10.3389/fnut.2024.1447878
24. HE J，YANG Y，ZHANG F，et al，Effects of Poria cocos extract on metabolic dysfunction-associated fatty liver disease via the FXR/PPARα-SREBPs pathway [J]，Front Pharmacol，2022，13，1007274.http://dx.doi.org/10.3389/fphar.2022.1007274
25. PATHAK P，XIE C，NICHOLS R G，et al，Intestine farnesoid X receptor agonist and the gut microbiota activate G-protein bile acid receptor-1 signaling to improve metabolism [J]，Hepatology，2018，68，4，，1574-1588.http://dx.doi.org/10.1002/hep.29857
26. ZHOU X，LI Y，YANG Y，et al，Regulatory effects of Poria cocos polysaccharides on gut microbiota and metabolites: evaluation of prebiotic potential [J]，NPJ Sci Food，2025，9，1，，53.http://dx.doi.org/10.1038/s41538-025-00416-9
27. HARTMANN P，HOCHRATH K，HORVATH A，et al，Modulation of the intestinal bile acid/farnesoid X receptor/fibroblast growth factor 15 axis improves alcoholic liver disease in mice [J]，Hepatology，2018，67，6，，2150-2166.http://dx.doi.org/10.1002/hep.29676
28. KANEHISA M，GOTO S，KEGG: Kyoto Encyclopedia of Genes and Genomes [J]，Nucleic Acids Res，2000，28，1，，27-30.http://dx.doi.org/10.1093/nar/28.1.27

Figures

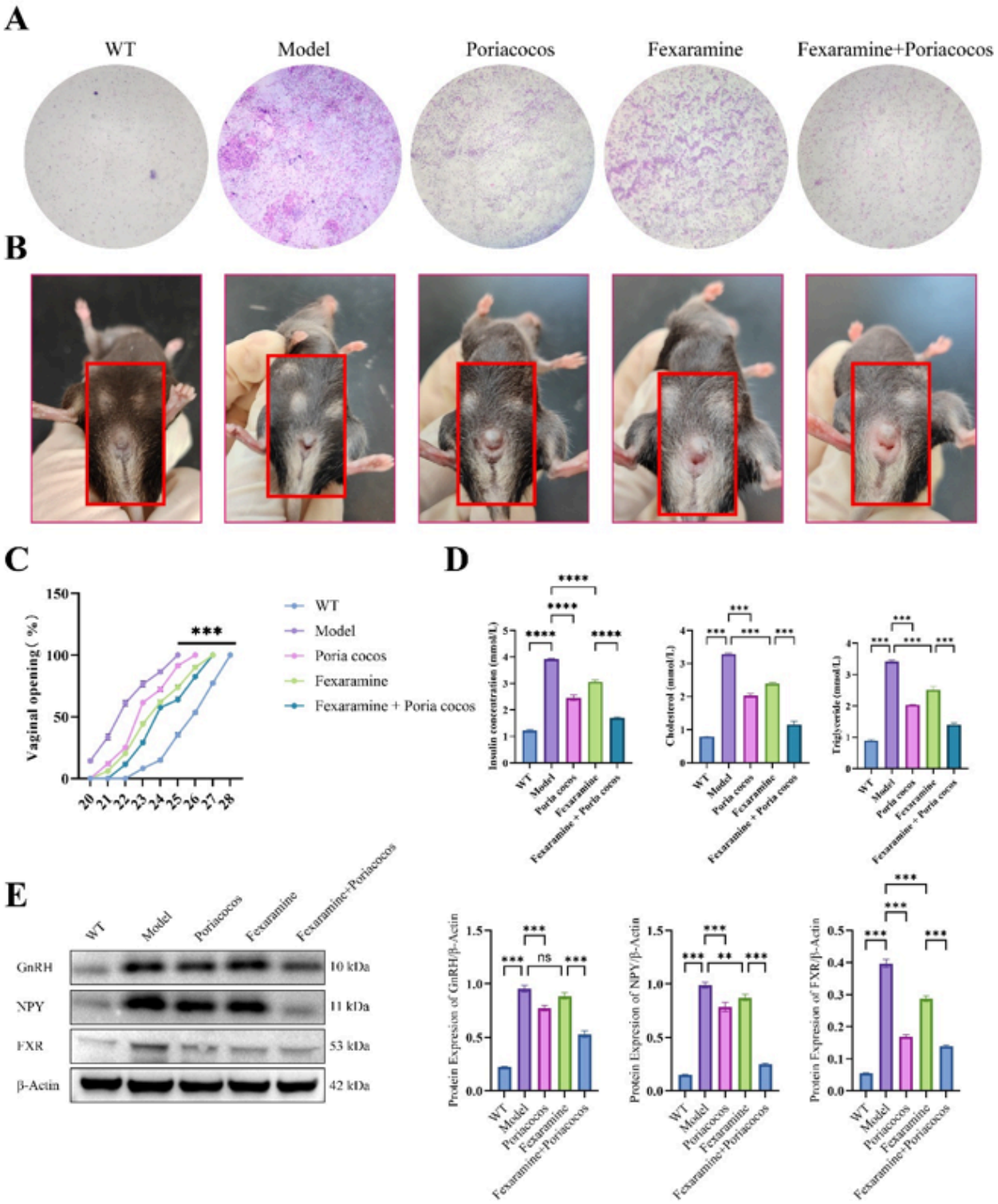


Figure 1

Pubertal timing, endocrine–metabolic readouts, and FXR/GnRH/NPY expression under HFD and interventions. (A) Representative vaginal-smear cytology on the day of VO for WT, Model (HFD), Poria cocos, Fexaramine, and Fexaramine+ Poria cocos groups; (B) Representative external genital images at VO for the same groups; (C) Cumulative VO curves (Kaplan–Meier) from postnatal day 21 onward; (D) Serum insulin and total Cholesterol (mmol L^{-1}). Bars show mean ± SD (n = 5 per group). Statistics: one-

way ANOVA with Tukey post hoc test unless indicated; p < 0.05, *p < 0.01, **p < 0.001, ***p < 0.0001; (E) Representative Western blots of hypothalamic GnRH and NPY and ileal FXR with β-actin as a loading control. Blots were cropped for presentation. Full-length.

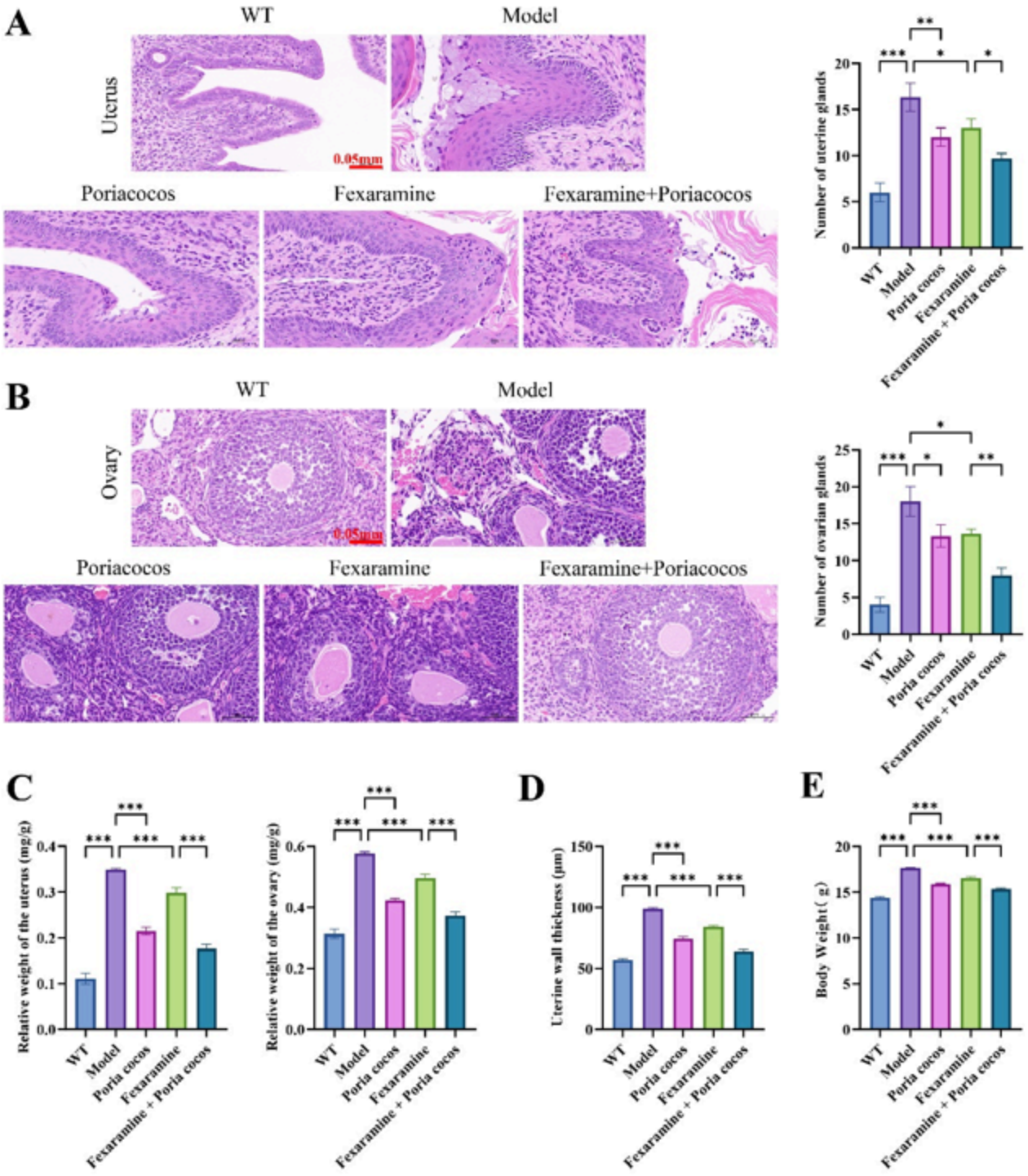


Figure 2

Reproductive histopathology and quantitative morphometrics under HFD and interventions. (A) Representative uterine H&E sections from WT, Model (HFD), Poria cocos, Fexaramine, and Fexaramine + Poria cocos groups, showing epithelial architecture and stromal features (scale bars, as indicated); (B)

Representative ovarian H&E sections from the same groups illustrating follicular/cystic morphology and stromal changes; (C) Uterine wall thickness (μm); (D) Relative uterine weight (mg g^{-1} body weight); (E) Relative ovarian weight (mg g^{-1} body weight); (F) Body weight (g). Bars represent mean ± SD (n = 5 per group). Statistics: one-way ANOVA with Tukey's post-hoc test unless otherwise specified; $p < 0.05$, *$p < 0.01$, **$p < 0.001$, ***$p < 0.0001$;

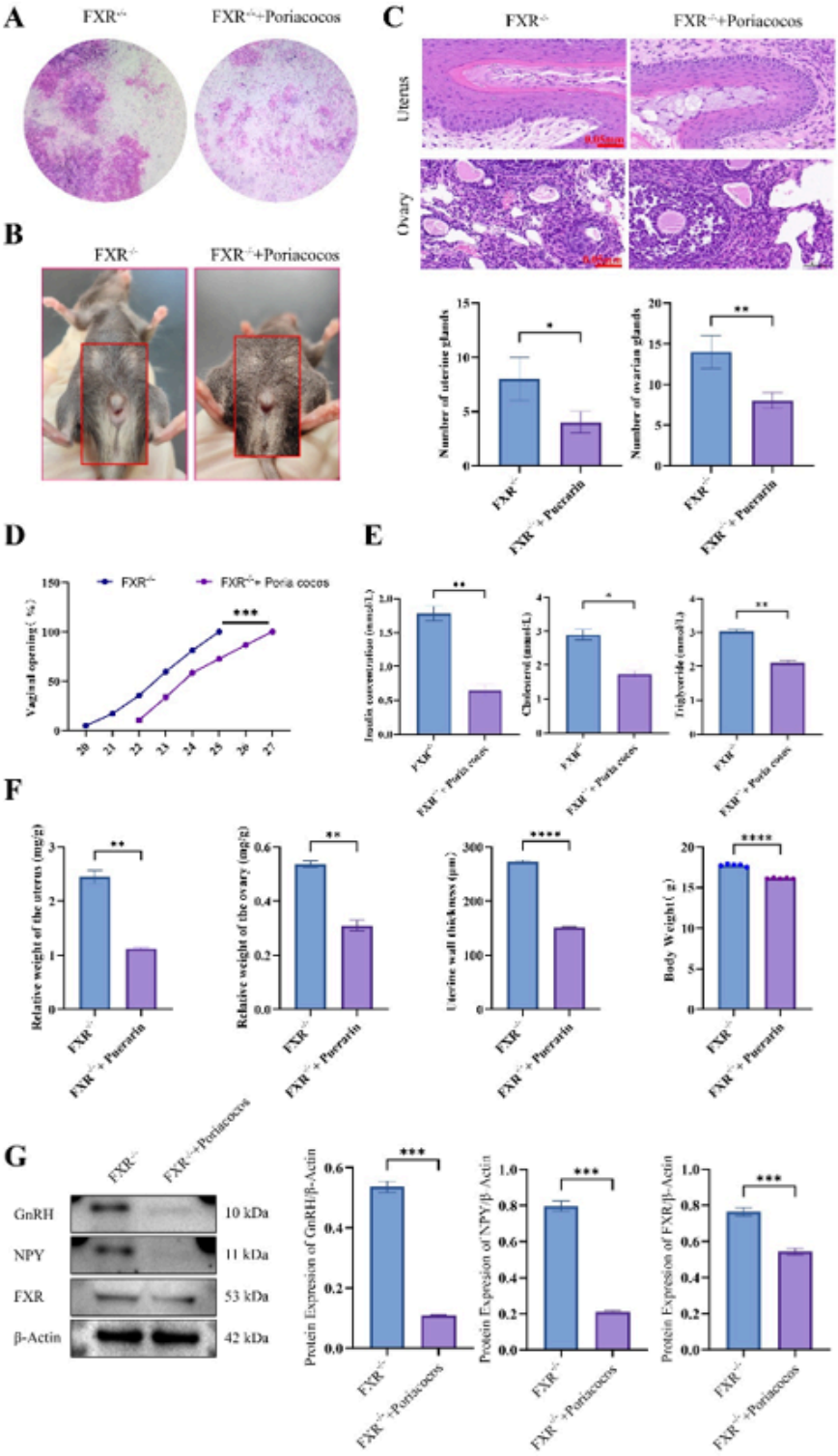


Figure 3

Readouts in $FXR^{-/-}$ mice with or without Poria cocos. (A) Representative vaginal-smear cytology on the day of VO ; (B) External genital photographs for $FXR^{-/-}$ and $FXR^{-/-}$ + Poria cocos groups; (C) Representative H&E sections of uterus and ovary for the same groups (scale bars shown on images); (D) Cumulative VO curves (Kaplan–Meier) from postnatal day 21; y-axis denotes the percentage of animals reaching VO; (E) Serum insulin, total cholesterol and triglycerides (mmol L^{-1}); bars depict mean ± SD (n = 5 per group); (F) Quantitative morphometrics: relative uterine weight and relative ovarian weight (mg g^{-1} body weight) and body weight (g); definitions and calculation methods as indicated in Methods; (G)Western blots for hypothalamic GnRH and NPY and ileal FXR with β-actin as a loading control. Blots were cropped for presentation. Full-length; densitometric quantification to be presented in accompanying bar graphs. Statistical tests planned: one-way ANOVA with Tukey’s post-hoc comparisons unless otherwise specified.

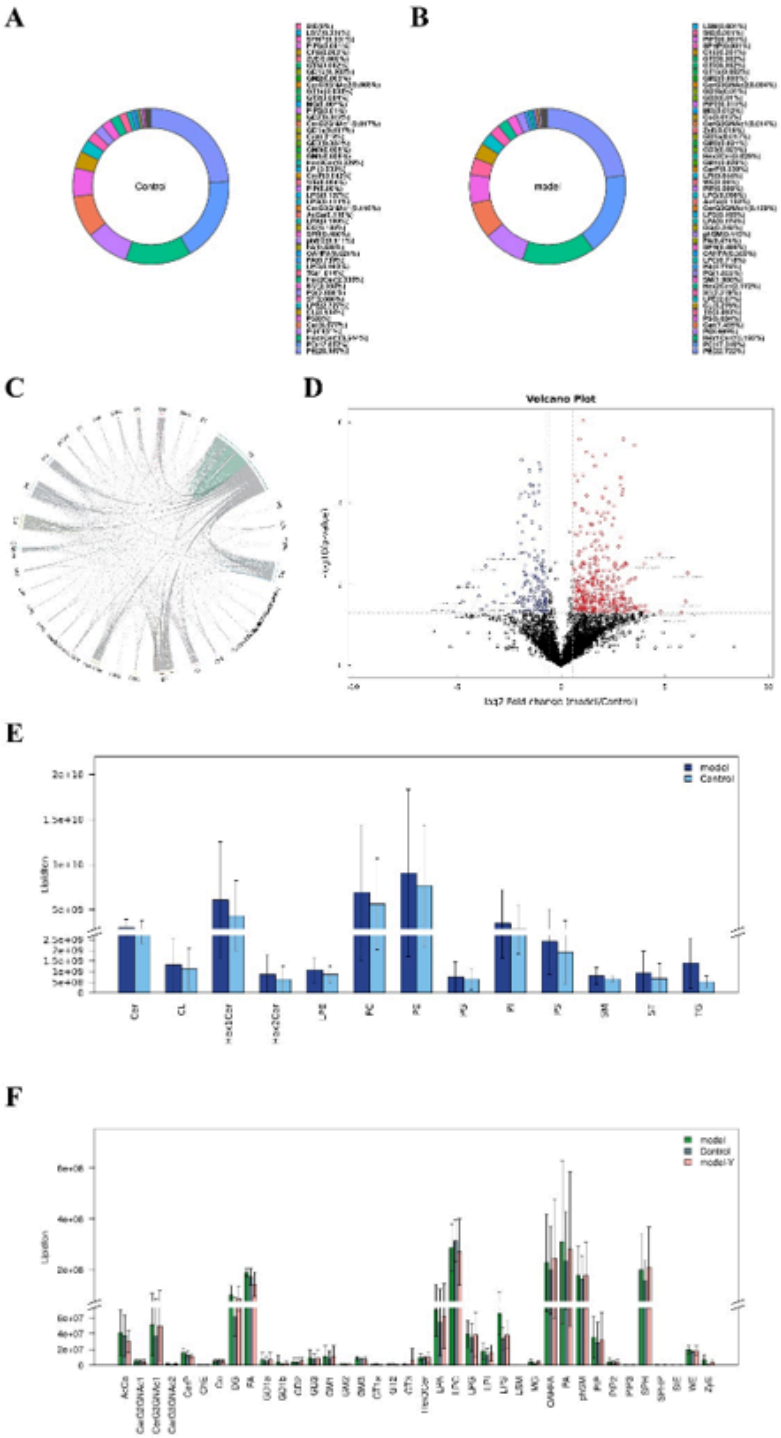


Figure 4

Lipidomic composition and network analyses. (A–B) Donut charts showing lipid subclass composition for Control and Model; (C) correlation/chord network of lipid subclasses/species; (D) volcano plot of differential lipid species for Model versus Control; (E) bar plot of absolute abundances for major lipid subclasses comparing Model and Control; (F) bar plot of selected lipid classes/species across Model, Control and model-Y.

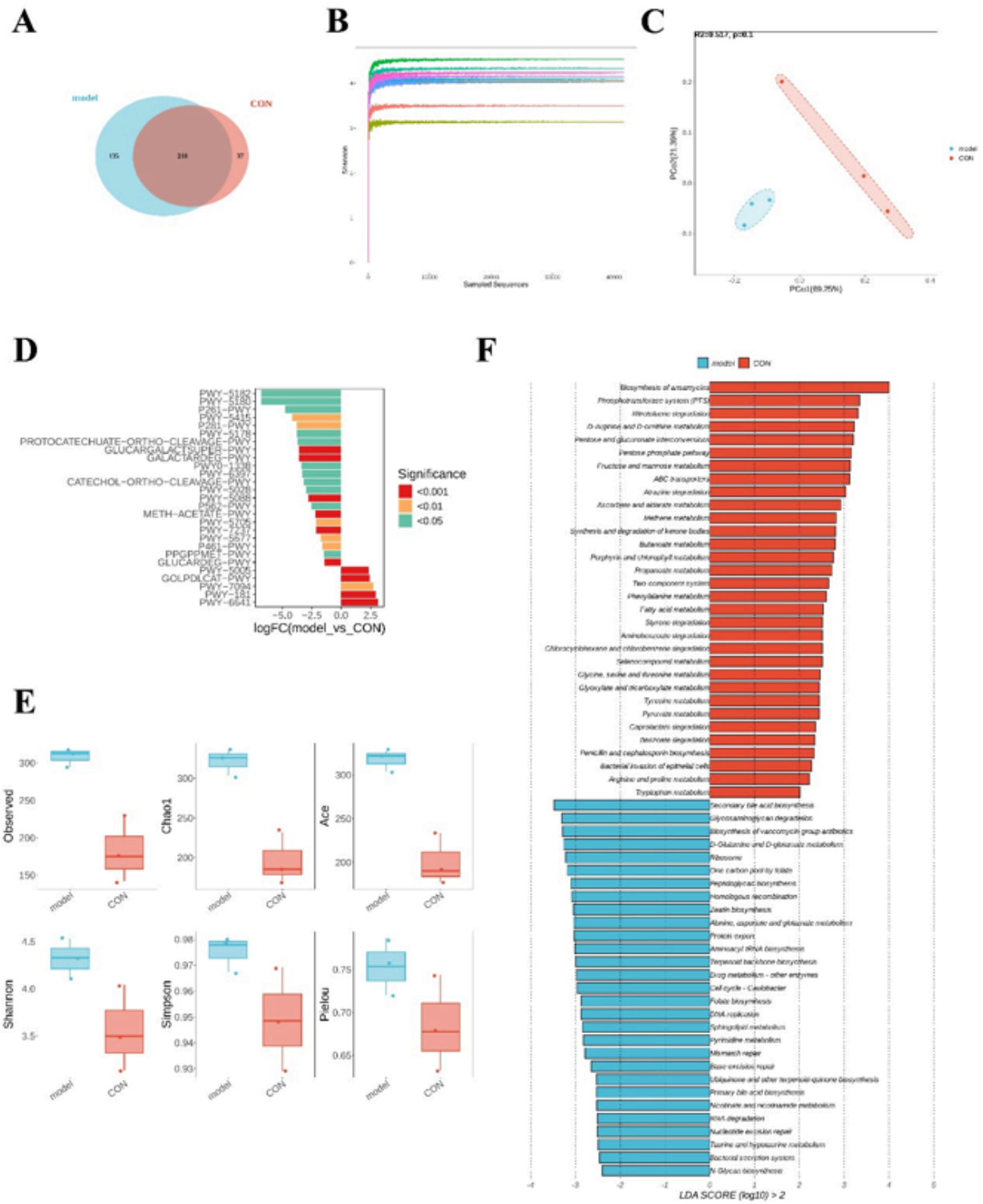


Figure 5

Microbiome composition, α/β-diversity and functional profiling. (A) Venn diagram of shared and unique amplicon sequence variants (ASVs) between Model and Control; (B) Shannon rarefaction curves versus sequencing depth; (C) principal coordinates analysis (PCoA) of β-diversity (Bray–Curtis or UniFrac) with 95% confidence ellipses; (D) LEfSe LDA bar plot of KEGG pathway enrichment (Kyoto Encyclopedia of Genes and Genomes, KEGG) (threshold as indicated)[28]; (E) differential pathway analysis for Model

versus Control shown as log fold change (logFC); (F) α-diversity boxplots for Observed richness, Chao1, ACE, Shannon, Simpson and Pielou indices.

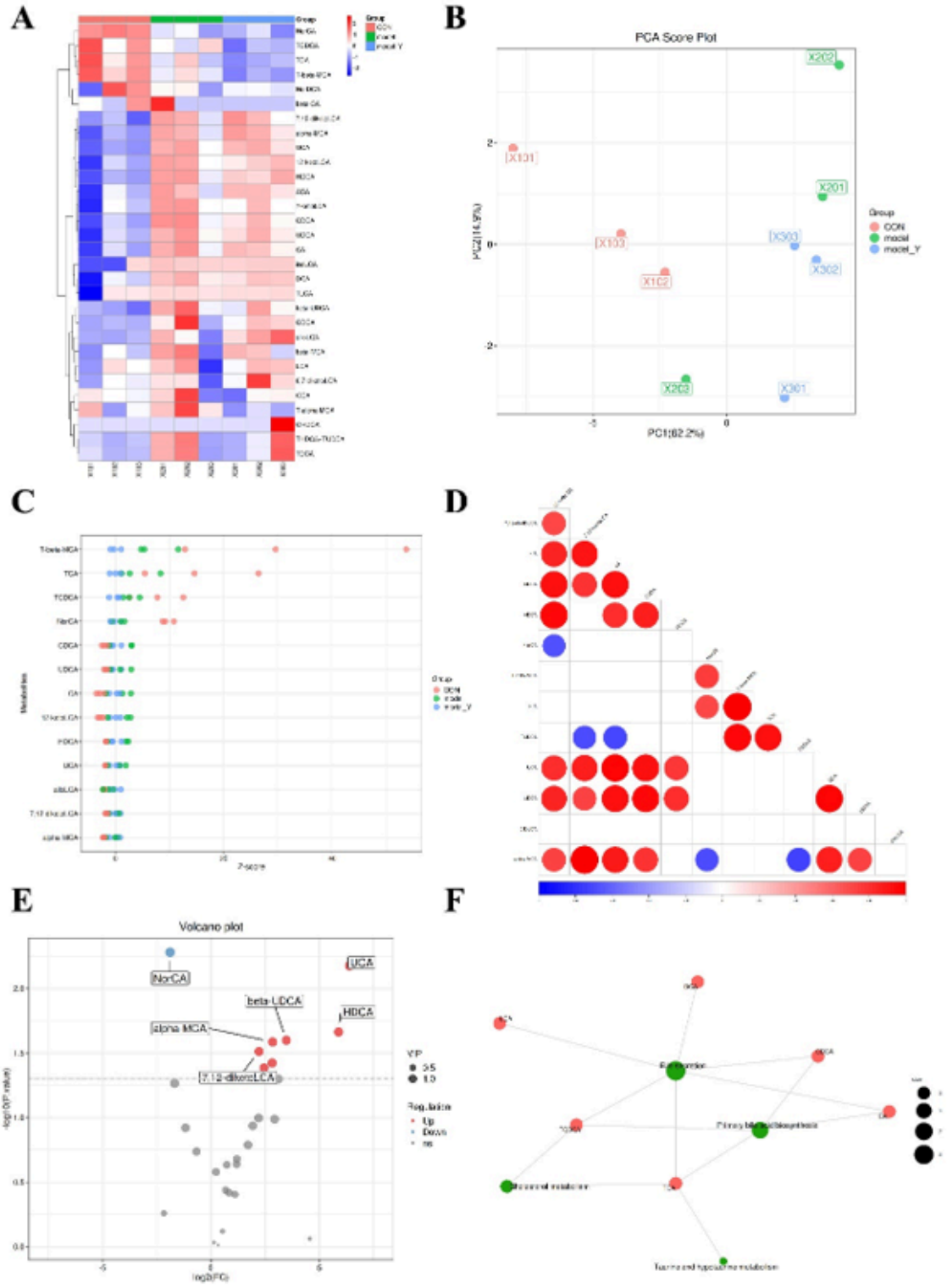


Figure 6

Bile-acid profiling and pathway mapping. (A) Hierarchical clustering heat map (Z-scores) of bile-acid species across Control (CON), Model and model_Y groups; (B) principal-component analysis (PCA) score plot with group colours and 95% confidence ellipses; (C) Z-score scatter of selected bile acids (labels as

shown); (D) pairwise correlation matrix (bubble plot) of bile-acid species (bubble size reflects |correlation|, colour denotes sign); (E) volcano plot for Model versus Control (log_2 fold change vs $-log_{10}$ P; point size encodes VIP; colour indicates up/down/non-significant classification); (F) Pathway network linking differential bile acids to KEGG pathways (Kyoto Encyclopedia of Genes and Genomes, KEGG) ; KEGG is copyright © Kanehisa Laboratories and is reproduced/adapted with permission.

Supplementary Files

This is a list of supplementary files associated with this preprint. Click to download.

- supplementaryfile.pdf